ARMY RESEARCH LABORATORY

Spatially Varying Aperture Weighting for Sidelobe Reduction and Resolution Enhancement of Imagery

by John W. McCorkle and Matthew Bennett

ARL-TR-1662 October 1998

The findings in this report are not to be construed as an official Department of the Army position unless so designated by other authorized documents.

Citation of manufacturer's or trade names does not constitute an official endorsement or approval of the use thereof.

Destroy this report when it is no longer needed. Do not return it to the originator.

Army Research Laboratory
Adelphi, MD 20783-1197

ARL-TR-1662 **October 1998**

Spatially Varying Aperture Weighting for Sidelobe Reduction and Resolution Enhancement of Imagery

John W. McCorkle and Matthew Bennett
Sensors and Electron Devices Directorate

Abstract

Synthetic aperture radar (SAR) engineers continue to search for algorithms and techniques that reduce sidelobes and improve the resolution of a given data set. The classical estimation of the power spectrum of a signal from a finite record of data is typically made using a discrete Fourier transform (DFT). To mitigate errors due to the data record being finite, one typically applies various windows (or apodizations) before transformation. These windows fall into two categories: raised cosine-based (e.g., Hanning, Hamming, Blackman-Harris, and Nutall windows), and noncosine-based (e.g., Dolph-Chebyshev, Taylor, Kaiser, and Gaussian windows). These windows trade off resolving power for improved (reduced) sidelobes. Similarly, SAR imagery exhibits sidelobes because the images are derived from a finite aperture. The same windows are applied to SAR data to reduce the sidelobes. This report describes a method of allowing a raised cosine-based window to be adaptively changed at each output data point (or pixel). The technique is spatially variant apodization (SVA). This spatially adaptive window maintains the resolution normally associated with rectangular weighting. However, it simultaneously reduces the sidelobes commensurate with the order of the filter (i.e., the number of cosine terms used). Results are shown on imagery from the U.S. Army Research Laboratory's ultra-wideband Boom-SAR system. It is important to note that SVA is not limited to SAR applications. It is applied in the image domain and is applicable to all systems that produce images.

Contents

Figures

1. Introduction

Synthetic aperture radar (SAR) integrates energy over a finite aperture to create pixel values in the output image. For a uniform (rectangular) weighting function across the aperture, the impulse response (IPR) for a point target return in one dimension is a sinc function. The closest sidelobe is 13.5 dB below the peak, and the sidelobe envelope decreases 6 dB/octave. Because the ultra-wideband (UWB) SAR imagery can have a large dynamic range, the sinc function sidelobes from a strong target can easily obscure weaker, nearby targets. To mitigate errors due to the data record being finite, one typically applies various windows (or apodizations) before transformation. These windows fall into two categories: raised cosine-based (e.g., Hanning, Hamming, Blackman-Harris, Taylor, and Nutall windows [1]), and noncosine-based (e.g., Dolph-Chebyshev and Kaiser windows). With the Hamming window, for example, the peak sidelobe is 43 dB below the peak of the response. This lower sidelobe comes at the cost of a main lobe that is 1.36 times wider, as compared to uniform, or rectangular, weighting.

Classical super-resolution techniques, such as Capons' minimum variance method (MVM), ESPRIT, and MUSIC (multiple signal classification), are based on an assumed model and estimates of the parameters of the model given the observed data. The solution of the system of equations required in these techniques is computationally burdensome. Compared with MVM, spatially variant apodization (SVA) does not require inversion of the covariance matrix. Also, estimating model orders is not trivial, and SVA has none to estimate. Jung and Munson [2] have shown that one-dimensional (1-D) SVA is a special version of the MVM.

SVA is the technique that optimizes the IPR on a point-by-point basis to minimize sidelobes in the SAR imagery. Stankwitz and others [3,4] introduced the 1-D SVA in 1994. It is an extension of dual apodization, which generates two images using two different normalized windows, and takes the output pixel from whichever image has the minimum absolute value. In this report, we extend these results to a full 2-D optimization. We describe several techniques that obtain high resolution and low sidelobes. They are simple to compute and do not assume a model. Instead, they allow a sum-of-raised-cosines-based window to be adaptively changed at each output data point (or pixel) to minimize sidelobe responses. This adaptive window maintains the resolution normally associated with rectangular weighting, yet simultaneously reduces the sidelobes commensurate with the order of the window (i.e., the number of cosine terms used).

Historically, SVA has referred to the special case where the window is a single raised cosine and where the cost function is minimum energy in the output pixel given a constrained region of weights spanning from uniform weighting to a Hanning window. Given the derivation of the SVA, DeGraaf [5,6] introduced the adaptive sidelobe reduction (ASR) algorithm. It uses the more general sum-of-raised-cosines window, and a

cost function constraint to handle the overdetermined parameter space. That cost function simply constrained the energy in the weights. A technique to apply SVA multiple times to obtain super-resolution has also been described by Stankwitz and Kosek [7].

None of the previous papers addresses using the algorithm on ultra-wide-bandwidth/ultra-wide-angle (UWB/UWA) SAR data. The derivations were based on narrow angle assumptions (i.e., down-range and cross-range sidelobes are orthogonal and lie on a Cartesian grid). We found, however, that the technique can be applied to UWB/UWA data with 90° integration angles. More recently, Rau and McClellan [8] have shown that applying a wedge-shaped window to the 2-D Fourier transform of a UWB image is nearly equivalent to applying a sliding (constant integration angle) window to the raw UWB/UWA SAR data. The result is valid for constant integration angle, strip-map mode focusing processes. In other words, a focusing process that produces an image with a spatially invariant IPR. The approximation used to obtain this result is accurate for the large 90° integration angles used in foliage penetration (FOPEN) SAR. Therefore, optimizing SVA to the UWA case requires the SVA sample spacing to be wedge-shaped (see eq (3)). Fixing R for small image chips has been found to produce excellent results.

Figure 1 shows the operations involved with image formation and how SVA is applied. An aperture weighting is typically applied in the raw data domain, as shown in the Aperture window 1 box. Instead of applying it there, Rau and McClellan showed that an angle-space window could be applied in the (k_x, k_y) domain, shown as the Aperture window 2 box. On the other side of the Fourier transform, this angle-space window can be applied using convolution instead of multiplication in the frequency domain. This position is naturally suitable for pixel-by-pixel optimization because forward and inverse Fourier transforms are unnecessary to test different windows. Furthermore, this position allows SVA to be applied to any image, regardless of how it was made. Therefore, it can be used to benefit more than just the SAR community.

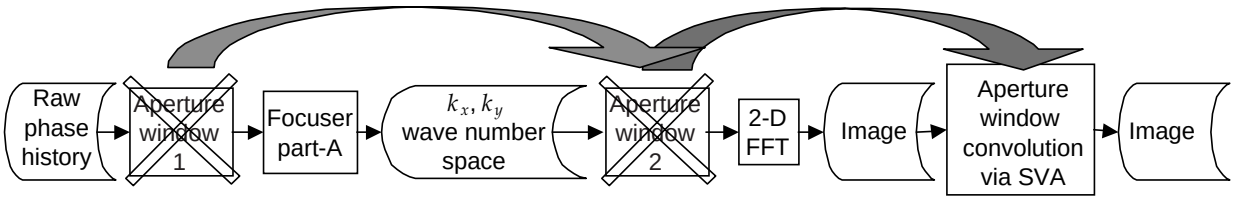

Figure 1. Image formation and application of SVA.

2. SVA Algorithm Description

First, we must define the sum-of-raised-cosines window. Let N be the number of points in an aperture, w be the variable parameter per second for the window, and $n = -N/2 \ldots N/2 - 1$. The raised cosine weighting functions are given by

$$A(n) = 1 + 2w_1 \cos\left(\frac{2\pi n}{N}\right) + 2w_2 \cos\left(\frac{4\pi n}{N}\right) + \ldots + 2w_k \cos\left(\frac{2k\pi n}{N}\right) . \quad (1)$$

For example, the family of first-order weighting functions ranges from uniform ($w_1 = 0$) to Hamming ($w_1 = 0.426$) to Hanning ($w_1 = 0.5$). A Blackman-Harris window is second-order with $w_1 = 110/189$, and $w_2 = 715/7938$.

The SVA algorithm is derived by the following argument. First, with the raised-cosine windows defined as above, the integral or summation across the aperture weights is independent of all w. Therefore, a unit point scatterer (amplitude = 1), will always focus to the same amplitude, regardless of all w. This means that the w's can be adjusted to minimize the amplitude of an output pixel because the w's cannot affect the amplitude of the desired point scatterer. The result is that sidelobes from other targets (i.e., at positions other than the desired output data point or pixel) are minimized.

For example, if we limited ourselves to a finite set of M w-vectors, SVA would be equivalent to focusing the image M times, once for each w-vector, and then letting each pixel in the output image equal the minimum (for the same pixel-position) from the M images produced by the M apodizations. Such a mechanization, of course, would require too much computation to be practical.

To make the approach practical, we first recall that multiplying by the raised cosine window in the (k_x, k_y) domain (i.e., the 2-D Fourier transform of the image) is equivalent to doing convolution in the image domain. Taking the length-N the discrete Fourier transform (DFT) of the raised cosine windowing function $A(n)$ yields the Nyquist-sampled IPR:

$$a(m) = w_k\delta_{m,-k} + \ldots + w_1\delta_{m,-1} + \delta_{m,0} + w_1\delta_{m,1} + \ldots + w_k\delta_{m,k} , \quad (2)$$

where $\delta_{m,k}$ is the Kronecker delta function $\delta_{m,k}\begin{cases} 1, & m = k \\ 0, & m \neq k \end{cases}$.

Thus, a first-order raised cosine windowing function IPR contains only three nonzero terms; namely $a(m) = w_1\delta_{m,-1} + \delta_{m,0} + w_1\delta_{m,1}$. This windowing function can be implemented efficiently using a three-point convolution in the image domain on complex Nyquist-sampled imagery that was generated with a uniform window. If the image is oversampled at, say, R times the Nyquist rate, then equation (2) becomes

$$a(m) = w_k\delta_{m,-kR} + \ldots + w_1\delta_{m,-R} + \delta_{m,0} + w_1\delta_{m,R} + \ldots + w_k\delta_{m,kR} . \quad (3)$$

R in equation (3) can be made proportional to range to produce the wedge-shaped window described by Rau and McClellan [8].

Next we must compute the optimum weights for each output point (or pixel). The 1-D SVA technique above must be modified to apply to the 2-D SAR imagery. The SVA can be applied in two ways: sequentially in 1-D, first on one axis and then upon the other, or in 2-D simultaneously. The sequential approach has the disadvantage of not being able to guarantee that the data provided to the second application of the SVA form an unambiguously Nyquist-sampled image because some points have been set to zero. Therefore, it may no longer be a smooth or band-limited function. The effect was used by Stankwitz and Kosek [7] to obtain superresolution.

Application of the SVA on the two dimensions simultaneously uses the following 2-D IPR:

$$\begin{pmatrix} w_m w_n & w_n & w_m w_n \\ w_m & 1 & w_m \\ w_m w_n & w_n & w_m w_n \end{pmatrix} . \tag{4}$$

We will now derive the optimum weights. Let the complex pixel value of the original unweighted image be defined as

$$g(m, n) = g_r(m, n) + jg_i(m, n). \tag{5}$$

Let $g'(m,n)$ be the output pixel in the reduced sidelobe image, and let

$$\begin{aligned} Q_m &= g(m-1, n) + g(m+1, n) \ , \\ Q_n &= g(m, n-1) + g(m, n+1) \ , \text{ and} \\ P_{m,n} &= g(m-1, n-1) + g(m+1, n+1) + g(m-1, n+1) + g(m+1, n-1) \ . \end{aligned} \tag{6}$$

At pixel (m, n) the sequential convolution of the 1-D IPR shown in equation (2) with the original unweighted image is given by

$$\breve{g}(m, n) = g(m, n) + w_n Q_n \text{ and } g'(m, n) = \breve{g}(m, n) + w_m Q_m \ . \tag{7}$$

At pixel (m, n), the convolution of the 2-D IPR shown in equation (4) with the original unweighted image is given by

$$g'(m, n) = g(m, n) + w_m w_n P_{m,n} + w_m Q_m + w_n Q_n. \tag{8}$$

We wish to minimize $|g'(m, n)|^2$ as a function of (w_m, w_n) subject to the constraints $0 \le w_m \le \frac{1}{2}$ and $0 \le w_n \le \frac{1}{2}$. These constraints force the window to lie between a uniform window ($w = 0$) and a Hanning window ($w = 0.5$). Without these constraints, the output pixel value would always be driven to zero. With this background, we now derive optimizations for four cases. We will use I, Q in the headings to mean the in-phase and quadrature components, which are the real and imaginary components, respectively.

2.1 Case 1: I, Q Separately and 2-D Coupled Weights

Although this derivation is provided by Stankwitz and others [4], it is repeated here for completeness. Consider the 2-D case where $w_m = w_n = w$ (i.e., the weightings in the two dimensions are coupled), and where $g(m, n)$ is either the real or the imaginary component of the image. The operations are carried out separately on the real and imaginary images. Let $Q_{m,n} = Q_m + Q_n$, where Q_m and Q_n are defined in equation (6). In this case, equation (8) becomes

$$g'(m, n) = g(m, n) + w^2 P_{m,n} + w Q_{m,n} \quad . \tag{9}$$

Local extrema in $g'^2(m, n)$ occur at the values of w for which $\frac{\partial g'^2(m, n)}{\partial w}$ = 0, which are given by

$$w = \begin{cases} \dfrac{-Q_{m,n} \pm \sqrt{Q_{m,n}^2 - 4P_{m,n}\, g(m, n)}}{2P_{m,n}} ; & \text{for } Q_{m,n}^2 - 4P_{m,n}\, g(m, n) > 0 \\ \dfrac{-Q_{m,n}}{2P_{m,n}} ; & \text{otherwise} \quad . \end{cases} \tag{10}$$

Noting that $g'(m, n) = w^2 P_{m,n} + w Q_{m,n} = -Q^2_{m,n}/4P_{m,n}$ for the otherwise case, the output pixel is then computed by the following rule:

$$g'(m, n) = \begin{cases} 0 ; & \text{if there are two } w \text{ and either lies in the interval } [0, \tfrac{1}{2}] , \\ g(m, n) - Q^2_{m,n}/4P_{m,n} ; & \text{if there is a single } w \text{ in the interval } [0, \tfrac{1}{2}] , \\ g(m, n) + w^2 P_{m,n} + w Q_{m,n}; & \text{where } w = \arg \min_{w \ni J} \left(\left| g(m, n) + w_m P_{m,n} + w Q_{m,n} \right| \right) , \text{ and} \\ J = \{0, 0.5\} ; & \text{otherwise} \quad . \end{cases} \tag{11}$$

2.2 Case 2: I, Q Separately and 2-D Uncoupled Weights

By allowing $w_m \neq w_n$, the two dimensions can be uncoupled. The derivation of the solution follows the same steps. Again, the operations are carried out separately on the real and imaginary images. Local extrema in $g'^2(m, n)$ occur at the values of w_m for which $\frac{\partial g'^2(m, n)}{\partial w_m}$ or $g'^2(m, n) = 0$, which is given by

$$(w_m, w_n) = \left(\frac{-Q_n}{P_{m,n}} , \frac{-Q_m}{P_{m,n}} \right) \text{ and} \tag{12}$$

$$w_m = \frac{-(w_n Q_n + g(m, n))}{w_n P_{m,n} + Q_m} \text{ or } w_n = \frac{-(w_m Q_m + g(m, n))}{w_m P_{m,n} + Q_m} \quad . \tag{13}$$

Solving equation (13) for the possible endpoints of a curve passing through the constraining box [0…½, 0…½], we get a set J_1 defined in equation (14). Tossing points outside the constraining box results in set J_2. If there is a sloping valley running across the constraining box, J_2 will not be empty. If J_2 is empty, then the corner points must be tested to find the minimum. We construct a set J containing the test points of interest as

$$J_1 = \left\{ \left(\frac{-(2g(m,n) + Q_n)}{P + 2Q_m}, \tfrac{1}{2} \right), \left(\frac{-g(m,n)}{Q_m}, 0 \right) \left(0, \frac{-g(m,n)}{Q_m} \right) \left(\tfrac{1}{2}, \frac{-(2g(m,n) + Q_m)}{P + 2Q_n} \right) \right\}$$

$$J_2 = J_1 \cap \{0 \ldots \tfrac{1}{2}\} \tag{14}$$

$$J = \begin{cases} J_2 ; & \text{if } J_2 \neq \{\text{empty}\} \\ \{(0,0), (0,0.5), (0.5,0), (0.5,0.5)\} ; & \text{otherwise} \end{cases} .$$

Now we can solve for the output. If from equation (11) $g'(m,n)$, then no more work is necessary. Otherwise, if (w_m, w_n) from equation (12) are both in the interval $[0, \frac{1}{2}]$, then they can be used directly in equation (8). If they are not, then the set J from equation (14) is computed. The output point is then computed as

$$\begin{aligned} g'(m,n) &= g(m,n) + w_m w_n P_{m,n} + w_m Q_m + w_n Q_n \ , \\ \text{where } (w_m, w_n) &= \arg \min_{(w_m, w_n) \in J} \left(\left| g(m,n) + w_m w_n P_{m,n} + w_m Q_m + w_n Q_n \right| \right) . \end{aligned} \tag{15}$$

2.3 Case 3: I, Q Jointly and 2-D Coupled Weights

Now we let $w_m = w_n$ and compute the optimum weight for the complex data, instead of separately operating on the real and imaginary parts. We will drop m and n for compactness. Subscripts r and i indicate the real and imaginary parts, respectively. Local extrema in $|g'(m,n)|^2$ occur at the values of w_m for which $\frac{\partial |g'(m,n)|^2}{\partial w_m} = 0$, or $|g'(m,n)|^2 = 0$. This results in the following cubic equation:

$$w^3 + \frac{3}{2} \frac{P_r Q_r + P_i Q_i}{P_r^2 + P_i^2} w^2 + \frac{2\left(P_r g_r + P_i g_i\right) + \left(Q_r^2 + Q_i^2\right)}{2\left(P_r^2 + P_i^2\right)} w + \frac{Q_r g_r + Q_i g_i}{2\left(P_r^2 + P_i^2\right)} = 0 \ . \tag{16}$$

This equation can be put into the form $x^3 + ax + b = 0$ by making the substitution

$$w = x - \frac{P_r Q_r + P_i Q_i}{2\left(P_r^2 + P_i^2\right)} \text{ , where } a = \frac{2(P_r g_r + P_i g_i) + \left(Q_r^2 + Q_i^2\right)}{2\left(P_r^2 + P_i^2\right)} - \left(\frac{P_r Q_r + P_i Q_i}{6\left(P_r^2 + P_i^2\right)} \right)^2 \text{ , and}$$

$$b = \frac{1}{4} \left(\frac{P_r Q_r + P_i Q_i}{P_r^2 + P_i^2} \right)^3 + \frac{(P_r Q_r + P_i Q_i)\left(2(P_r g_r + P_i g_i) + \left(Q_r^2 + Q_i^2\right)\right)}{4\left(P_r^2 + P_i^2\right)^2} + \frac{Q_r g_r + Q_i g_i}{2\left(P_r^2 + P_i^2\right)} \ . \tag{17}$$

For the solution, we let

$$c = \sqrt[3]{-\frac{b}{2} + \sqrt{\frac{b^2}{4} + \frac{a^3}{27}}} \text{ , and } d = \sqrt[3]{-\frac{b}{2} - \sqrt{\frac{b^2}{4} + \frac{a^3}{27}}} \quad , \tag{18}$$

and the solutions for w are

$$\begin{aligned} w &= \left[c + d - \frac{P_r Q_r + P_i Q_i}{2\left(P_r^2 + P_i^2\right)} \right] , \\ &= \left[\frac{c-d}{2}\sqrt{-3} - \frac{c+d}{2} - \frac{P_r Q_r + P_i Q_i}{2\left(P_r^2 + P_i^2\right)} \right] , \text{ and} \\ &= \left[-\frac{c-d}{2}\sqrt{-3} - \frac{c+d}{2} - \frac{P_r Q_r + P_i Q_i}{2\left(P_r^2 + P_i^2\right)} \right] . \end{aligned} \tag{19}$$

The following conditions apply to the roots.

If $\frac{b^2}{4} + \frac{a^3}{27} > 0$, there will be one real root and two conjugate imaginary roots.

If $\frac{b^2}{4} + \frac{a^3}{27} = 0$, there will be three real roots, of which at least two are equal.

If $\frac{b^2}{4} + \frac{a^3}{27} < 0$, there will be three real unequal roots.

We construct a set J as follows:

$$\begin{aligned} J_1 &= \{\text{all real roots}\} \cap \{0 \ldots ½\} \\ J &= \begin{cases} J_1 ; & \text{if } J_1 \neq \{\text{empty}\} \\ \{(0, 0), (0, 0.5), (0.5, 0), (0.5, 0.5)\}; & \text{otherwise} \end{cases} . \end{aligned} \tag{20}$$

The complex output point is then computed with the complex data using

$$g'(m, n) = g(m, n) + w^2 P_{m,n} + wQ \, , \tag{21}$$

where $w = \arg \min_{w \in J} \left(\left| g(m, n) + w^2 P_{m,n} + wQ \right| \right)$.

2.4 Case 4: I, Q Jointly and 2-D Uncoupled Weights

Now we let $w_m \neq w_n$ and compute the optimum weight for the complex data, instead of separately operating on the real and imaginary parts.

Local extrema in $\left| g'(m, n) \right|^2$ occur at the values of w_m for which

$\frac{\partial \left| g'(m, n) \right|^2}{\partial w_m} = 0$ and $\frac{\partial \left| g'(m, n) \right|^2}{\partial w_n} = 0$, or $\left| g'(m, n) \right|^2 = 0$. Unlike the other

cases, the resulting simultaneous equations could not be solved. Consequently, an iterative algorithm is used to find the minimum. The solution to the two partial derivatives results in

$$w_m = \frac{-(w_n^2(P_rQ_{nr} + P_iQ_{ni}) + w_n(P_rg_r + P_ig_i + Q_{mr}Q_{nr} + Q_{mi}Q_{ni}) + Q_{mr}g_r + Q_{mi}g_i)}{w_n^2(P_r^2 + P_i^2) + 2w_n(P_rQ_{mr} + P_iQ_{mi}) + Q_{mr}^2 + Q_{mi}^2} \quad , \tag{22}$$

and

$$w_n = \frac{-(w_m^2(P_rQ_{mr} + P_iQ_{mi}) + w_m(P_rg_r + P_ig_i + Q_{mr}Q_{nr} + Q_{mi}Q_{ni}) + Q_{nr}g_r + Q_{ni}g_i)}{w_m^2(P_r^2 + P_i^2) + 2w_m(P_rQ_{nr} + P_iQ_{ni}) + Q_{nr}^2 + Q_{ni}^2} \quad . \tag{23}$$

The solution for $|g'(m, n)|^2 = 0$ can be put into the form $aw_n^2 + bw_n + c = 0$, where

$$\begin{aligned} a &= w_m^2(P_r^2 + P_i^2) + 2w_m(P_rQ_{nr} + P_iQ_{ni}) + Q_{nr}^2 + Q_{ni}^2 \ , \\ b &= 2(w_m^2(P_rQ_{mr} + P_iQ_{mi}) + w_m(P_rg_r + P_ig_i + Q_{mr}Q_{nr} + Q_{mi}Q_{ni}) + Q_{nr}g_r + Q_{ni}g_i) \text{ , and} \\ c &= w_m^2(Q_{mr}^2 + Q_{mi}^2) + 2w_m(Q_{mr}g_r + Q_{mi}g_i) + g_r^2 + g_i^2 \ . \end{aligned} \tag{24}$$

This solution—depending on the relative size of a, b, and c—has the roots of

$$R_1 = \frac{-b - \text{sgn}(b)\sqrt{b^2 - 4ac}}{2a} \text{ and } R_2 = \frac{c}{aR_1} \text{ , or} \tag{25}$$

$$R_1 = \frac{-2c}{-b - \text{sgn}(b)\sqrt{b^2 - 4ac}} \text{ and } R_2 = \frac{c}{aR_1} \quad . \tag{26}$$

For example if $c \approx 0$, then equation (25) is better conditioned. But if $a \approx 0$, then equation (26) is better conditioned and R_2 can be ignored. A real root is required for $g'(m,n) = 0$. Thus, for w_n in the interval $[0 \ldots ½]$, if $b^2 - 4ac \geq 0$ (i.e., real roots) and either root is in the interval $[0 \ldots ½]$, then $g'(m, n) = 0$. Otherwise, use equation (23) to find an interval

$$H_n = [0 \ldots ½, w_n] \cap [0 \ldots ½, 0 \ldots ½] \quad . \tag{27}$$

Use equation (22) to find an interval

$$H_m = [w_n, 0 \ldots ½] \cap [0 \ldots ½, 0 \ldots ½] \quad . \tag{28}$$

If both exist, then let

$$J = \{(w_m, w_n)\} = H_m \cup H_n \ , \tag{29}$$

where J is now the optimum weights. If only H_n exists, then let

$$J = \{(0, w_n), (½, w_n)\} \in H_m \quad . \tag{30}$$

If only H_m exists, then let

$$J = \{(w_m, 0), (w_m, ½)\} \in H_m \quad . \tag{31}$$

If neither set exists, then let

$$J = \{(0, 0), (0, 0.5), (0.5, 0), (0.5, 0.5)\} \ . \tag{32}$$

The solution is then found with equation (15).

3. ASR Algorithm

The ASR algorithm takes SVA to higher order and uses a different constraint. To go to higher order, we let the single weight w_m grow to N_m weights with the notation ${}^k w_m$, where $k = 1 \ldots N_m$. Similarly, we let the single weight w_n grow to N_n weights with the notation ${}^p w_n$, where $p = 1 \ldots N_n$. ASR adopts the constraint

$$\sum_{k=1}^{N_m} {}^k w_m^2 + \sum_{p=1}^{N_n} {}^p w_n^2 \le c \ , \tag{33}$$

where c is chosen arbitrarily by the user. In other words, if equation (33) is met where the minimum occurs, then the minimum is used. If equation (33) is not met where the minimum occurs, then a new minimum is found where the sum of the squares of the weights exactly equals c, and this minimum is used. Like the SVA, if no constraint was used, then the weights would always force the output to zero. This new constraint, however, has no good physical basis—it is just mathematically convenient.

Along with Behboodian, Reise, and McClellan [9], we have found that the application of the ASR algorithm to UWB/UWA SAR data is not as helpful as SVA because ASR attacks large targets.

3.1 Physical Explanation for Poor Performance

There is a simple physical reason, never discussed in the literature, why higher order SVA and ASR would have difficulty attacking large targets. Namely, large targets are not isotropic. Instead, they typically have large backscatter over a few degrees of angular space. This is due to the specular response off the side of the target as the SAR passes. The derivation of SVA assumed an isotropic scatterer, and set up the weights such that the isotropic target could not be attacked. With a first-order filter, the freedom to attack a nonisotropic scatterer is very small. The results bear this out. With higher orders, however, and especially with the constraint used with ASR, there is great freedom to attack large targets. While this paper does not cover derivation and implementation of another constraint, we recommend that future work be directed along four approaches.

3.2 Proposed Solution for the Poor Performance

We propose four ways to mitigate the poor performance. First, the present constraint could be weighted, as in

$$\sum_{k=1}^{N_m} {}^k w_m^2 \, W_k + \sum_{p=1}^{N_n} {}^p w_n^2 \, W_p \le c \ , \tag{34}$$

Here, W could be made monotonically increasing to force the higher order terms to smaller values. This would be consistent with known good windows such as Nutall windows.

Second, the present constraint could be modified to limit how far the solution can move away from a known good window. For example, let $\psi = \{{}^1w_i, {}^2w_i, {}^3w_i, \ldots\}$ be the ideal coefficients for a Nutall window, and let $W = \left\{ \frac{1}{{}^1w^\alpha}, \frac{1}{{}^2w^\alpha}, \frac{1}{{}^3w^\alpha}, \ldots \right\}$, where a good α is probably 2. Then the constraint would be

$$\sum_{k=1}^{N_m} ({}^kw_m - {}^kw_i)^2 W_k + \sum_{p=1}^{N_n} ({}^pw_n - {}^pw_i)^2 W_p \le c \quad . \tag{35}$$

Third, the present constraint could be simply replaced in the computer with a nonlinear iterative procedure that constrained each term to a range from 0 to a limit; for example, $\beta\psi$, where β is slightly larger than 1. This would be most like the first-order SVA that constrains the solution to fall between uniform and Hanning weighting.

Fourth, as will be seen in the results section, application of SVA to an image that was previously weighted effectively raises the order of the overall filter. For example, two three-tap convolutions can be duplicated with a single five-tap convolution. Therefore, SVA could be applied to cases of the original data, data modified by a Hamming window, and data modified by a Blackman window. Then the overall minimum can be taken as the output pixel.

These four approaches would limit the ability of the variable apodization window to place a dip in the region where a large target has its high specular lobe. At the same time, they would allow a higher order window to be applied. Therefore, better sidelobe performance would be expected.

3.3 Taking Advantage of the Problem for ATD Purposes

The problem could be turned around for use in an automatic target detector. In general, manmade targets have flat surfaces that produce specular lobes. Therefore, the window could be constructed specifically to allow the flexibility to produce a dip where the response from a large target could fall. For example, () could be changed to

$$A(n) = 1 + 2w_1 \cos\left(\frac{2\pi n}{N} + \theta_1\right) + 2w_2 \cos\left(\frac{4\pi n}{N} + \theta_2\right) + \ldots + 2w_k \cos\left(\frac{2k\pi n}{N} + \theta_n\right) \quad . \tag{36}$$

A detector could then be trained (e.g., a neural net or a polynomial detector) to observe the coefficients and generate detections.

4. Results on Actual SAR Data

We evaluated the algorithms using data from the U.S. Army Research Laboratory (ARL) BoomSAR system. The image chip selected for analysis contains a corner reflector as well as vehicles and trees, which provide canonical IPRs. Figure 2 shows the image created using uniform weighting. Figure 3 shows the image created using Hamming weighting. These provide a baseline and show the sidelobe reduction and resolution reduction available with a classic window. Figure 4 shows an image after applying SVA to the uniform windowed image. It shows that very significant improvements are gained through SVA. The resolution is equal to figure 2, yet its sidelobes are lower than figure 3. Figure 5 shows an image after applying SVA to the Hamming windowed image. As expected, the resolution does not equal that of figure 3. Nonetheless, there is noticeable improvement in the sidelobes. The sidelobe reduction provides greater detail in the resulting image. Figure 6 shows the effect of applying the ASR algorithm to the Hamming-weighted image. Figure 7 is a plot showing the cross-range profiles for four cases: Hamming, uniform, SVA-on-Hamming, and SVA-on-uniform. Figure 8 is a plot showing the down-range profiles for the four cases. Figure 7 does not fully capture the effectiveness of the SVA algorithm because the cross-range sidelobes lie at an angle to the down-range, cross-range grid (i.e., they appear as an "X" in fig. 2). Nonetheless, the figures show that the SVA has reduced the sidelobes by over 10 dB, relative to classic Hamming weighting.

It is interesting to note that the SVA applied to a Hamming-weighted image sometimes outperforms the SVA applied to a uniformly weighted image. At first, this occurrence may seem unexpected because the SVA-on-uniform "should have been optimal." However, by prewindowing with the Hamming weight, the SVA is now effectively applying a five-tap filter to the uniform image instead of a three-tap filter. This result argues that a higher order filter will further improve performance.

As mentioned previously, the ASR algorithm allows a higher order filter, but the cost function for ASR appears to have problems. We found, along with Behboudian and others [9], that large targets were distorted by the ASR algorithm. Object size, however, is one of the important features used in automatic target detection (ATD) for FOPEN targets. Application of the SVA to the Hamming-weighted image shows the utility of the fourth method proposed in section 3.2 for mitigating ASR's attack on large targets.

Figure 2. Corner reflector image using uniform weighting.

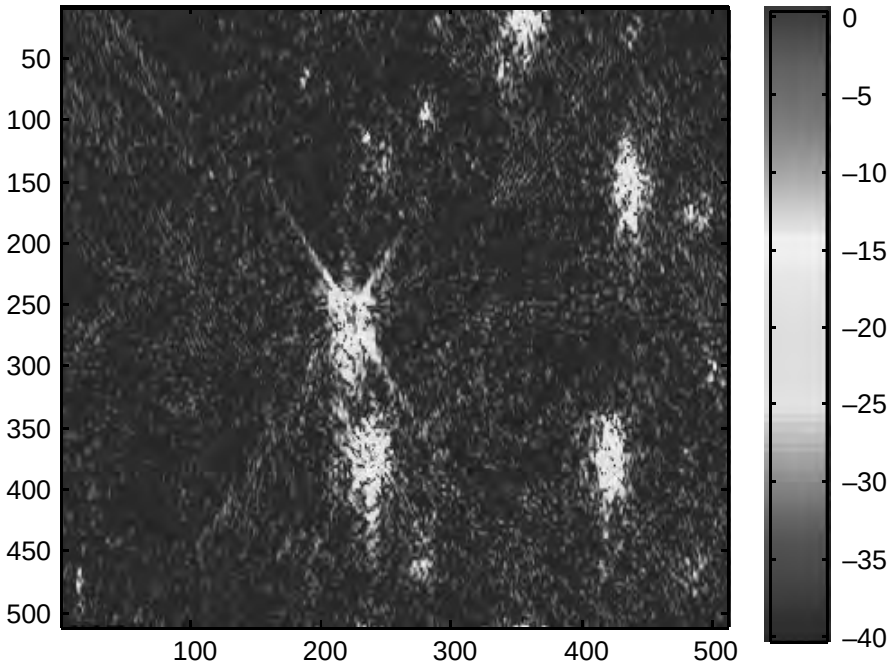

Figure 3. Corner reflector image using Hamming weighting.

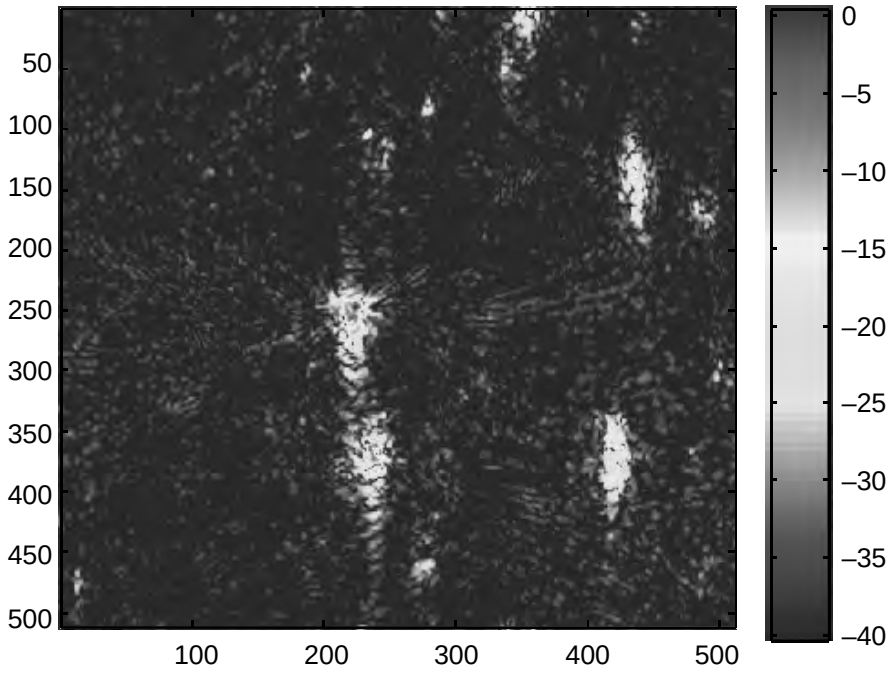

Figure 4. Corner reflector image after applying SVA to the uniform windowed image.

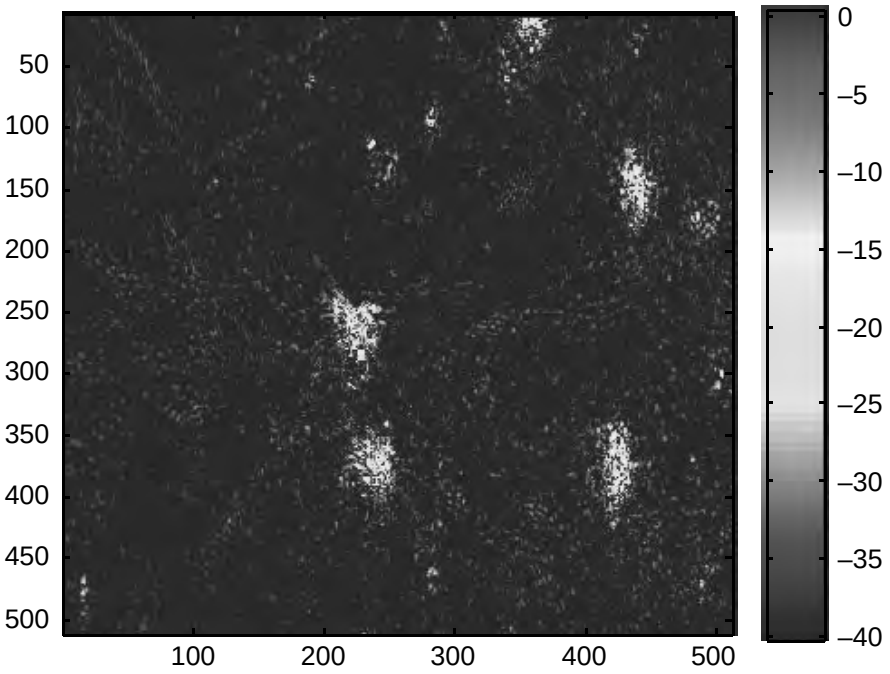

Figure 5. Corner reflector image after applying SVA to the Hamming windowed image.

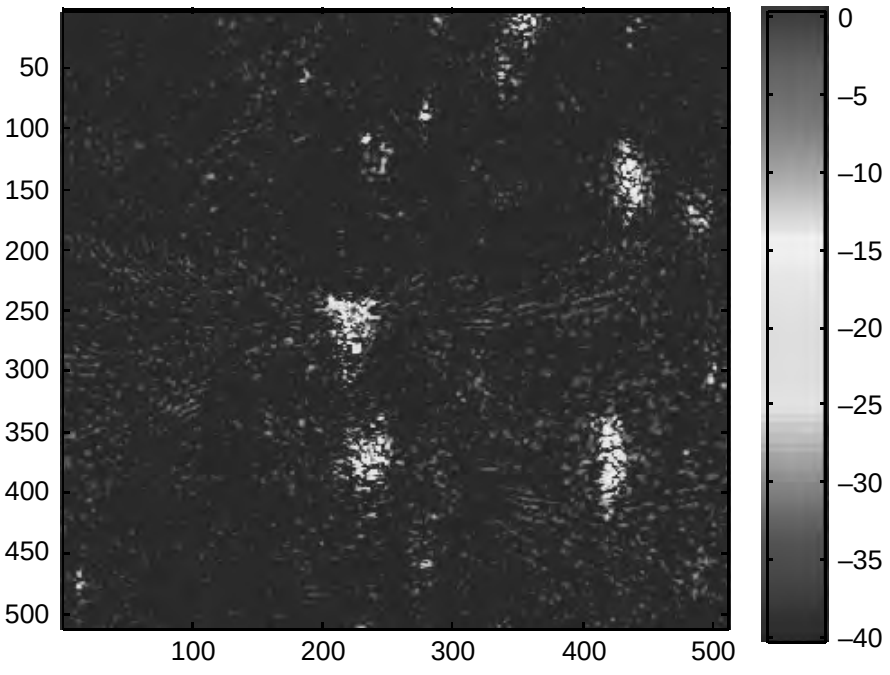

Figure 6. Corner reflector image after applying ASR to the Hamming windowed image.

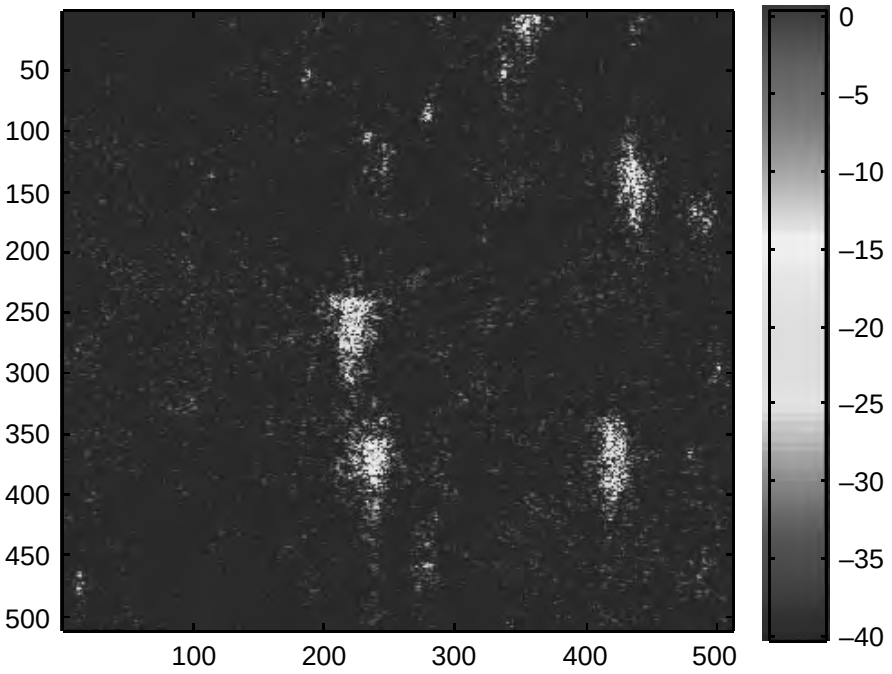

Figure 7. Cross-range profiles for Hamming, uniform, SVA-on-Hamming, and SVA-on-uniform windows.

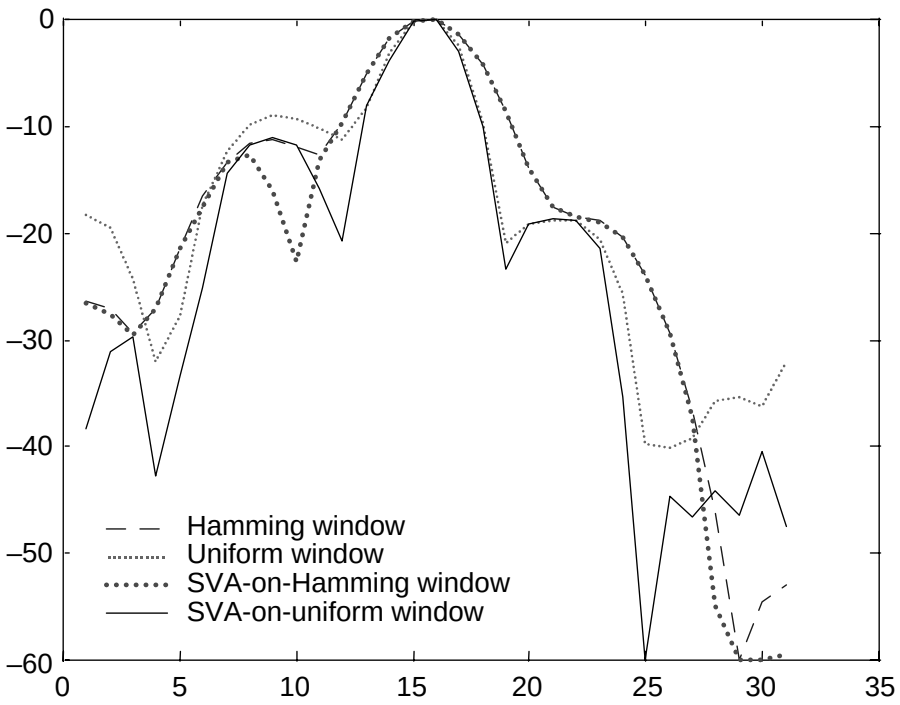

Figure 8. Down-range profiles for Hamming, uniform, SVA-on-Hamming, and SVA-on-uniform windows.

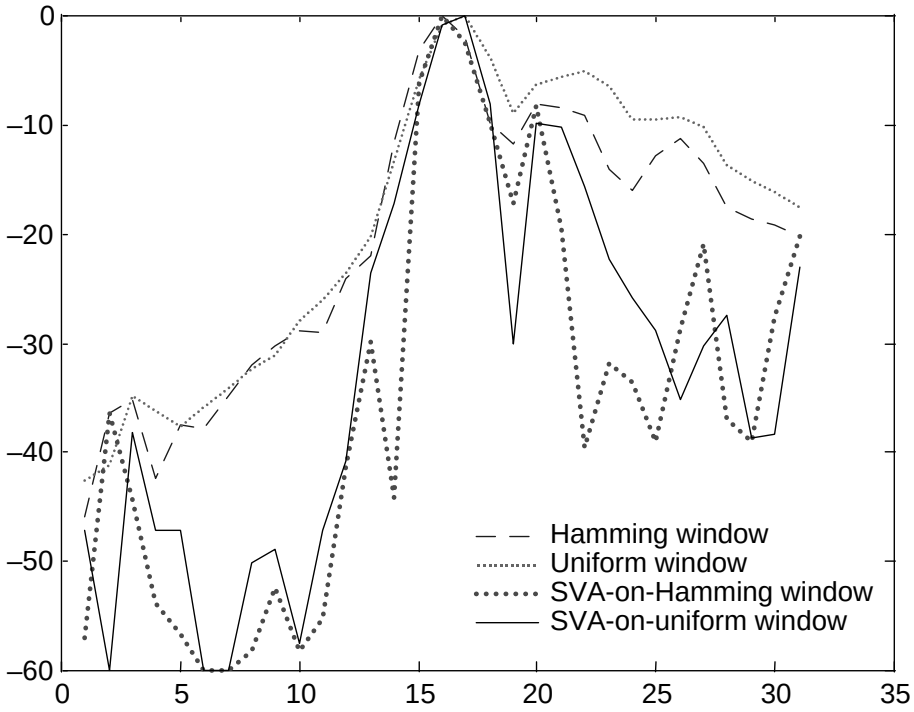

5. Conclusions and Future Work

We have derived optimizations for four 2-D cases of first-order SVA, for cases for real and imaginary parts both separately and jointly, and for each of these with the 2-D weights both coupled and uncoupled. We reference material that indicates that SVA needs no additional complications to operate in the UWA domain, consistent with FOPEN SAR. Furthermore, we have shown that SVA is very effective on UWB/UWA images.

We obtained over 10 dB of sidelobe suppression without a reduction in resolution. The algorithm is capable of revealing to image analysts the small targets and signature aspects that were previously hidden by sidelobes. We expect the performance of automatic target detection and recognition (ATD/R) algorithms to significantly improve after application of SVA because the analysts will have access to information in images that was previously buried by sidelobes. If unsmoothed source data are available, then SVA can provide even greater gains because previously unresolved features may be resolved. Improved detection, classification, and recognition by both automated and human interpreters should result.

While ASR appeared to show promise, the cost function allows it to attack large targets. This action has deleterious effects on current FOPEN ATD algorithms. Most targets of interest for FOPEN applications are large.

We produced a physical explanation for this behavior. Based on these physics, we know that the key is in the cost function constraints. We proposed four alternative constraints that would limit the variable apodizations to be closer to known high-performance windows, such as a Blackman-Harris for second order and Nutall for higher order.

Unexpectedly, based on the physical explanation for the ASR algorithm for attacking large targets, we propose that advantage could be taken of this "drawback." We propose using it for ATD purposes. In this case, the form of the apodization window is specifically constructed to allow dips to occur. The window coefficients (as opposed to the image) are then fed to a trained detector as one part of the ATD processes.

6. References

1. A. Nutall, "Some Windows with Very Good Sidelobe Behavior," *IEEE Trans. Acoust. Speech Signal Process*. **ASSP-29** (February 1981), pp 84–91.
2. Jung Ah Choi Lee and David Munson, Jr., "Effectiveness of Spatial-Variant Apodization," *IEEE 1995 Proc., International Conf. on Image Processing* (1995), pp 147–150.
3. H. C. Stankwitz, R. J. Dallaire, and J. R. Fienup, "Spatially Variant Apodization for Sidelobe Control in SAR Imagery," *IEEE Record of the 1994 National Radar Conference* (1994), pp 132–137.
4. H. C. Stankwitz, R. J. Dallaire, and J. R. Fienup, "Nonlinear Apodization for Sidelobe Control in SAR Imagery," *IEEE Trans. AES*. **31**, 1 (January 1995), pp 267–279.
5. Stuart DeGraaf, "Sidelobe Reduction via Adaptive FIR Filtering in SAR Imagery," *IEEE Trans. Image Processing* **3**, 3 (May 1994), pp 292–301.
6. Stuart DeGraaf, "SAR Imaging via Spectral Estimation Methods," *IEEE 1994 Record of the 28th Asilomar Conf. on Signals, Systems, and Computers* (1994), pp 117–121.
7. H. C. Stankwitz and M. R. Kosek, "Sparse Aperture Fill for SAR Using Super-SVA," *IEEE 1996 Proc. National Radar Conf*. (1996), pp 70–75.
8. Richard Rau and James McClellan, "Aspect Angle Information of Targets in UWB SAR Image and New Post Processing Techniques," *Advanced Sensors: Proceedings of the 2nd Annual FedLab Symposium* (sponsored by the Army Research Laboratory under cooperative agreement DAAL01-96-2-0002), College Park, MD (2–6 February 1998), pp 127–131.
9. A. Behboodian, F. Reise, and J. McClellan, "Adaptive Sidelobe Reduction for UWB SAR," *Advanced Sensors: Proceedings of the 2nd Annual FedLab Symposium* (sponsored by the Army Research Laboratory under cooperative agreement DAAL01-96-2-0002), College Park, MD (2–6 February 1998), pp 161–165.

Distribution

Admnstr
Defns Techl Info Ctr
Attn DTIC-OCP
8725 John J Kingman Rd Ste 0944
FT Belvoir VA 22060-6218

Ofc of the Dir Rsrch and Engrg
Attn R Menz
Pentagon Rm 3E1089
Washington DC 20301-3080

Ofc of the Secy of Defns
Attn ODDRE (R&AT) G Singley
Attn ODDRE (R&AT) S Gontarek
The Pentagon
Washington DC 20301-3080

OSD
Attn OUSD(A&T)/ODDDR&E(R) R J Trew
Washington DC 20301-7100

AMCOM MRDEC
Attn AMSMI-RD W C McCorkle
Redstone Arsenal AL 35898-5240

CECOM
Attn PM GPS COL S Young
FT Monmouth NJ 07703

Dir for MANPRINT
Ofc of the Deputy Chief of Staff for Prsnnl
Attn J Hiller
The Pentagon Rm 2C733
Washington DC 20301-0300

Hdqtrs Dept of the Army
Attn DAMO-FDT D Schmidt
400 Army Pentagon Rm 3C514
Washington DC 20301-0460

US Army Edgewood RDEC
Attn SCBRD-TD J Vervier
Aberdeen Proving Ground MD 21010-5423

US Army Info Sys Engrg Cmnd
Attn ASQB-OTD F Jenia
FT Huachuca AZ 85613-5300

US Army Natick RDEC Acting Techl Dir
Attn SSCNC-T P Brandler
Natick MA 01760-5002

US Army Rsrch Ofc
4300 S Miami Blvd
Research Triangle Park NC 27709

US Army Simulation, Train, & Instrmntn Cmnd
Attn J Stahl
12350 Research Parkway
Orlando FL 32826-3726

US Army Tank-Automtv & Armaments Cmnd
Attn AMSTA-AR-TD M Fisette
Bldg 1
Picatinny Arsenal NJ 07806-5000

US Army Tank-Automtv Cmnd Rsrch, Dev, & Engrg Ctr
Attn AMSTA-TA J Chapin
Warren MI 48397-5000

US Army Test & Eval Cmnd
Attn R G Pollard III
Aberdeen Proving Ground MD 21005-5055

US Army Train & Doctrine Cmnd
Battle Lab Integration & Techl Dirctrt
Attn ATCD-B J A Klevecz
FT Monroe VA 23651-5850

US Military Academy
Dept of Mathematical Sci
Attn MAM D Phillips
West Point NY 10996

Nav Surface Warfare Ctr
Attn Code B07 J Pennella
17320 Dahlgren Rd Bldg 1470 Rm 1101
Dahlgren VA 22448-5100

DARPA
Attn B Kaspar
3701 N Fairfax Dr
Arlington VA 22203-1714

University of Texas ARL Electromag Group
Attn Campus Mail Code F0250 A Tucker
Austin TX 78713-8029

Palisades Inst for Rsrch Svc Inc
Attn E Carr
1745 Jefferson Davis Hwy Ste 500
Arlington VA 22202-3402

Distribution (cont'd)

J McCorkle (5 copies)
8709 Oxwell La
Laurel MD 20708-2453

M Bennett (5 copies)
5022 Dull Knife Dr
Austin TX 78759

US Army Rsrch Lab
Attn AMSRL-CI-LL Techl Lib (3 copies)
Attn AMSRL-CS-AL-TA Mail & Records Mgmt
Attn AMSRL-CS-EA-TP Techl Pub (3 copies)
Attn AMSRL-SE-RU J Sichina
Attn AMSRL-SE-RU K Kappra
Adelphi MD 20783-1197

REPORT DOCUMENTATION PAGE

Form Approved
OMB No. 0704-0188

1. AGENCY USE ONLY *(Leave blank)*	2. REPORT DATE	3. REPORT TYPE AND DATES COVERED
	October 1998	Final, April to September 1997

4. TITLE AND SUBTITLE
Spatially Varying Aperture Weighting for Sidelobe Reduction and Resolution Enhancement of Imagery

5. FUNDING NUMBERS
DA PR: AH16
PE: 62120A

6. AUTHOR(S)
John W. McCorkle and Matthew Bennett

7. PERFORMING ORGANIZATION NAME(S) AND ADDRESS(ES)
U.S. Army Research Laboratory
Attn: AMSRL-SE-RU (hazmat@motor.arl.army.mil)
2800 Powder Mill Road
Adelphi, MD 20783-1197

8. PERFORMING ORGANIZATION REPORT NUMBER
ARL-TR-1662

9. SPONSORING/MONITORING AGENCY NAME(S) AND ADDRESS(ES)
U.S. Army Research Laboratory
2800 Powder Mill Road
Adelphi, MD 20783-1197

10. SPONSORING/MONITORING AGENCY REPORT NUMBER

11. SUPPLEMENTARY NOTES
AMS code: 622120.H16
ARL PR: 7NE41D

12a. DISTRIBUTION/AVAILABILITY STATEMENT
Approved for public release; distribution unlimited.

12b. DISTRIBUTION CODE

13. ABSTRACT *(Maximum 200 words)*

Synthetic aperture radar (SAR) engineers continue to search for algorithms and techniques that reduce sidelobes and improve the resolution of a given data set. The classical estimation of the power spectrum of a signal from a finite record of data is typically made using a discrete Fourier transform (DFT). To mitigate errors due to the data record being finite, one typically applies various windows (or apodizations) before transformation. These windows fall into two categories: raised cosine-based (e.g., Hanning, Hamming, Blackman-Harris, and Nutall windows), and noncosine-based (e.g., Dolph-Chebyshev, Taylor, Kaiser, and Gaussian windows). These windows trade off resolving power for improved (reduced) sidelobes. Similarly, SAR imagery exhibits sidelobes because the images are derived from a finite aperture. The same windows are applied to SAR data to reduce the sidelobes. This report describes a method of allowing a raised cosine-based window to be adaptively changed at each output data point (or pixel). The technique is spatially variant apodization (SVA). This spatially adaptive window maintains the resolution normally associated with rectangular weighting. However,

(continued on back)

14. SUBJECT TERMS
Spectral window, radar, SAR, super-resolution, SVA

15. NUMBER OF PAGES
28

16. PRICE CODE

17. SECURITY CLASSIFICATION OF REPORT	18. SECURITY CLASSIFICATION OF THIS PAGE	19. SECURITY CLASSIFICATION OF ABSTRACT	20. LIMITATION OF ABSTRACT
Unclassified	Unclassified	Unclassified	UL

NSN 7540-01-280-5500

Standard Form 298 (Rev. 2-89)
Prescribed by ANSI Std. Z39-18
298-102

13. Abstract (cont'd)

it simultaneously reduces the sidelobes commensurate with the order of the filter (i.e., the number of cosine terms used). Results are shown on imagery from the U.S. Army Research Laboratory's ultra-wideband Boom-SAR system. It is important to note that SVA is not limited to SAR applications. It is applied in the image domain and is applicable to all systems that produce images.

DEPARTMENT OF THE ARMY
U.S. Army Research Laboratory
2800 Powder Mill Road
Adelphi, MD 20783-1197